A memristor oscillator based on a twin-T network*

Li Zhi-Jun(李志军)[a)b)†] and Zeng Yi-Cheng(曾以成)[b)]

[a)] College of Information Engineering, Xiangtan University, Xiangtan 411105, China
[b)] Department of Optoelectronic Engineering, Xiangtan University, Xiangtan 411105, China

(Received 20 August 2012; revised manuscript received 21 September 2012)

A novel inductance-free nonlinear oscillator circuit with a single bifurcation parameter is presented in this paper. This circuit is composed of a twin-T oscillator, a passive RC network, and a flux-controlled memristor. With an increase in the control parameter, the circuit exhibits complicated chaotic behaviors from double periodicity. The dynamic properties of the circuit are demonstrated by means of equilibrium stability, Lyapunov exponent spectra, and bifurcation diagrams. In order to confirm the occurrence of chaotic behavior in the circuit, an analog realization of the piecewise-linear flux-controlled memristor is proposed, and Pspice simulation is conducted on the resulting circuit.

Keywords: chaos, memristor, piecewise-linear, twin-T oscillator

PACS: 05.45.–a **DOI:** 10.1088/1674-1056/22/4/040502

1. Introduction

The memristor, next to the resistor, the capacitor, and the inductor, was postulated as the fourth circuit element by Chua in 1971.[1] The memristor is defined as a two-terminal circuit element in which the flux ϕ between the terminals is a function of electric charge q that has passed through the device.[2] Researchers had not paid much attention to memristors for almost 40 years until Strukov *et al*.[3] fabricated a solid-state memristor using nanotechnology in 2008. Since the advent of memristors, a great deal of work has been reported in the science and engineering fields due to their unpredictable behaviors.[4] Thus far, research has demonstrated the promising applications of memristors, such as in resistive random access memory (RRAM) and logic modules in the digital realms.[5–7] In the case of analog computation, it has recently been shown that the memristor can simulate the processes typical of biological systems, such as the adaptive behavior of unicellular organisms, and learning and associative memory, and hence could be available in neuromorphic circuits.[8–10]

As a nonlinear circuit element at the nanoscale, the memristor is very suitable for realizing high-frequency chaotic oscillators, which have great potential applications in secure communication and image (or real-time video) encryption. Itoh and Chua[11] proposed several nonlinear memristor oscillators according to some of Chua's well studied circuits, in which the Chua diodes were replaced by the monotonically increasing piecewise-linear (PWL) memristors. Employing the same model, Muthuswary and Kokate[12] presented memristor-based chaotic circuits derived from the canonical Chua's circuit. Furthermore, some memristor-based oscillator schemes were introduced by replacing the nonlinear device in Chua's circuit with a monotonically increasing cubic function.[13–16] From the point of view of the circuit design, the chaotic circuit should be able to be implemented with electronic components. Since memristors are not yet commercially available, the dynamical behaviors of the above mentioned circuits were all investigated only by numerical simulation, except in the experimental study in Ref. [13], in which the authors introduced an analog realization of the monotone increasing cubic memristor and performed an experiment on the resulting circuit. Moreover, an issue worth paying attention to is that all of the above circuits contained an inductor, which made the circuits bulky, less robust, unsuitable for IC (integrated circuit) design, etc.

In this work, an inductor-free nonlinear oscillator composed of a twin-T oscillator, memristor, and RC network is designed. Unlike the other memristor-based chaotic circuits in Refs. [11]–[16], the novel chaotic circuit is inductance-free and hence has all the advantages of an inductance-free circuit (e.g. robustness, convenient for IC integration). Furthermore, the memristor is very suitable for dealing with high-frequency signals due to its nanoscale.[11] The purpose of employing a memristor as a nonlinear element is mainly to make the circuit ideal for applications related to high-frequency chaotic oscillators and secure communications. The proposed chaos circuit will exhibit complicated chaotic behaviors from double periodicity by changing the value of the transit capacitor. The dynamic properties of the new chaotic circuit are demonstrated by means of equilibrium stability, Lyapunov exponent spectra, and bifurcation diagrams. In order to confirm the chaotic behaviors of the circuit, Pspice simulation results obtained using a new emulator of the flux-controlled PWL memristor are included.

*Project supported by the National Natural Science Foundation of China (Grant Nos. 60972147 and 61176032).
†Corresponding author. E-mail: lizhijun@xtu.edu.cn
© 2013 Chinese Physical Society and IOP Publishing Ltd

2. Circuit description

The proposed circuit configuration is shown in Fig. 1, where a twin-T sinusoidal oscillator is coupled to a flux-controlled piecewise linear memristor via a passive RC network. The twin-T oscillator is the beating heart and provides energy to the chaos circuit. The memristor acts as a nonlinear element that makes the circuit variables abruptly change. Note that the operational amplifier serves as a voltage controlled voltage source (VCVS) with gain $k = 1 + R_4/R_5$. The symmetrical twin-T network satisfies the following restrictions: $R_1 = R_2 = 2R_3 = R_0$ and $C_1 = C_2 = 0.5C_3 = C_0$. In this study, we regard the flux-controlled memristor as a piecewise-linear nonlinear circuit element that is characterized by its nonlinear constitutive relation between flux ϕ and electric charge q

$$q(\varphi) = b\varphi + 0.5(a-b)(|\varphi+1| - |\varphi-1|). \tag{1}$$

In this case, its memductance function $W(\varphi)$ is defined as

$$W(\varphi) = \frac{\mathrm{d}q(\varphi)}{\mathrm{d}\varphi} = \begin{cases} a, & \text{if } |\varphi| < 1, \\ b, & \text{if } |\varphi| > 1, \end{cases} \tag{2}$$

representing the slope of the scalar function $q = q(\varphi)$. Accordingly, the relation between its terminal voltage v and the terminal current i can be expressed as

$$i = W(\varphi)v. \tag{3}$$

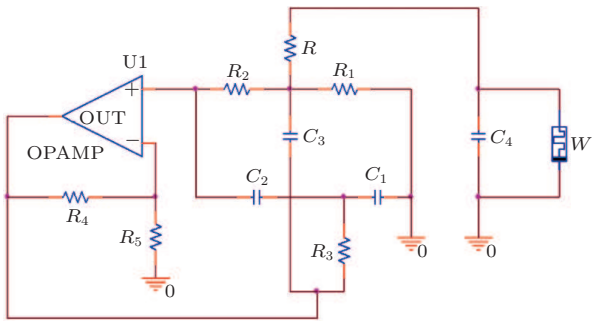


Fig. 1. (color online) Proposed chaos circuit with flux-controlled PWL memristor.

We can present the dynamics of the circuit by the following system of first-order differential equations:

$$\begin{cases} C_1\dfrac{\mathrm{d}v_{C_1}}{\mathrm{d}t} = C_2\dfrac{\mathrm{d}v_{C_2}}{\mathrm{d}t} - \dfrac{(1-k)v_{C_1} - kv_{C_2}}{R_3}, \\ C_2\dfrac{\mathrm{d}v_{C_2}}{\mathrm{d}t} = \dfrac{(k-1)(v_{C_1}+v_{C_2})+v_{C_3}}{R_2}, \\ -C_3\dfrac{\mathrm{d}v_{C_3}}{\mathrm{d}t} = \dfrac{k(v_{C_1}+v_{C_2})+v_{C_3}}{R_1} + C_2\dfrac{\mathrm{d}v_{C_2}}{\mathrm{d}t} \\ \qquad + \dfrac{k(v_{C_1}+v_{C_2})+v_{C_3}-v_{C_4}}{R}, \\ C_4\dfrac{\mathrm{d}v_{C_4}}{\mathrm{d}t} = \dfrac{k(v_{C_1}+v_{C_2})+v_{C_3}-v_{C_4}}{R} - W(\phi)v_{C_4}, \\ \dfrac{\mathrm{d}\phi}{\mathrm{d}t} = v_{C_4}. \end{cases} \tag{4}$$

By introducing the following variables and parameters: $x = v_{C_1}$, $y = v_{C_2}$, $z = v_{C_3}$, $w = v_{C_4}$, $u = \phi$, $\alpha = C_0/C_4$, and $\gamma = R_0/R$, letting R_0=1 and C_0=1, and combining the restrictions of the twin-T network, equation set (4) can be transformed into a dimensionless form as follows:

$$\begin{cases} \dot{x} = 3(k-1)x + (3k-1)y + z, \\ \dot{y} = (k-1)(x+y) + z, \\ -2\dot{z} = (2k-1+rk)(x+y) + (2+r)z - rw, \\ \dot{w} = \alpha\{r[k(x+y)+z-w] - W(u)w\}, \\ \dot{u} = w, \end{cases} \tag{5}$$

where

$$W(u) = \begin{cases} a, & \text{if } |u| < 1, \\ b, & \text{if } |u| > 1. \end{cases} \tag{6}$$

Choosing the parameters as $\alpha = 9$, $k = 1.05$, $\gamma = 2/3$, $a = -0.6$, and $b = 0.6$, and setting the initial conditions (0.01, 0, 0, 0, 0), the equilibrium point of the system (5) is obtained by equating the terms on the right-hand sides of Eq. (5) to zero, and is given by set $A = \{(x,y,z,w,u)|x = y = z = w = 0, u = \text{constant}\}$, which corresponds to the u-axis. The Jacobian matrix $\boldsymbol{J}$ at the equilibrium set can be expressed as

$$\boldsymbol{J} = \begin{bmatrix} 3(k-1) & 3k-1 & 1 & 0 & 0 \\ k-1 & k-1 & 1 & 0 & 0 \\ -\dfrac{2k-1+rk}{2} & -\dfrac{2k-1+rk}{2} & -\dfrac{2+r}{2} & \dfrac{r}{2} & 0 \\ \alpha rk & \alpha rk & \alpha r & -\alpha(r+W(u)) & 0 \\ 0 & 0 & 0 & 1 & 0 \end{bmatrix}, \tag{7}$$

and its characteristic equation is given by

$$|\lambda_i I - J| = 0. \tag{8}$$

The five eigenvalues of the equilibrium state (0, 0, 0, 0, constant) can be written as

$$\begin{cases} \lambda_1 = 0,\ \lambda_2 = -11.561,\ \lambda_3 = -1.066, & \\ \lambda_{4,5} = 0.047 \pm \mathrm{i}1.022, & \text{for } |u| < 1, \\ \lambda_1 = 0,\ \lambda_2 = 1.144,\ \lambda_3 = -1.7941, & \\ \lambda_{4,5} = -0.542 \pm \mathrm{i}1.081, & \text{for } |u| > 1. \end{cases} \tag{9}$$

Thus, they are characterized by an unstable saddle focus. The circuit performs chaotic behaviors, and a double-scroll is shown in Fig. 2. The corresponding Lyapunov exponents ($LE_1 = 0.073, LE_2 = 0, LE_3 = -0.002, LE_4 = -0.984, LE_5 = -10.126$) and Lyapunov dimension $d_{\rm L} = 3.076$ can be obtained from the sampled time series.

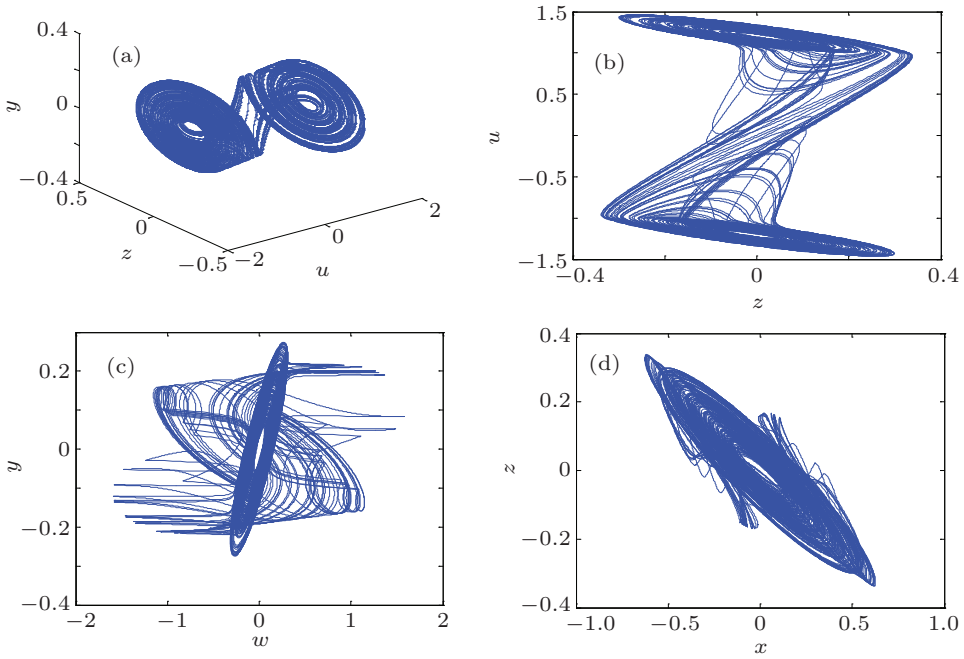


Fig. 2. (color online) Some typical chaotic attractors in (a) the u–z–y plane, (b) the z–u plane, (c) the w–y plane, and (d) the x–z plane.

3. Dynamical behaviors of the system

In this section, we further research the dynamical behaviors of the proposed chaos circuit with the aid of conventional dynamic analytical approaches, including dissipativity, Lyapunov exponents, and bifurcation diagrams.

3.1. Dissipativity

The state space of system (5) is five-dimensional, and the divergence of the vector field is easily calculated as

$$\begin{aligned}\nabla V &= \frac{\partial \dot{x}}{x} + \frac{\partial \dot{y}}{y} + \frac{\partial \dot{z}}{z} + \frac{\partial \dot{w}}{w} + \frac{\partial \dot{u}}{u} \\ &= 4(k-1) - \left(\frac{2+\gamma}{2}\right) - \alpha(\gamma + W(u)). \end{aligned} \tag{10}$$

According to Eq. (6), if $a = -0.6$, $b = 0.6$, $k = 1.05$, and $\gamma = 2/3$, then

$$\nabla V = \begin{cases} -\dfrac{1}{15}(17+\alpha), & \text{for } |u| < 1, \\ -\dfrac{1}{30}(17+38\alpha), & \text{for } |u| > 1. \end{cases} \tag{11}$$

So the system is always dissipative with a corresponding exponential contraction rate $e^{-(17+\alpha)/15}$ or $e^{-(17+38\alpha)/30}$ for any positive value α. That is, a volume element V_0 is contracted by the flow into a volume element $V_0 e^{-(17+\alpha)t/15}$ or $V_0 e^{-(17+38\alpha)t/30}$ at time t. This means that each volume containing the system orbit shrinks to zero as $t \to 0$. Therefore, all the trajectories of the system will be eventually confined to a subset that has zero volume, and the asymptotic motion will settle onto an attractor of the system.

3.2. Lyapunov exponents and bifurcation diagrams

The Lyapunov exponents and bifurcation diagrams are the effective measures for determining whether a system is chaotic. So we provide the corresponding Lyapunov exponent spectra of system (5), which is shown in Fig. 3. The bifurcation diagram is given in Fig. 4. In the numerical simulations, α acts as the control parameter, keeping the other parameters fixed at $k = 1.05$, $\gamma = 2/3$, $a = -0.6$, and $b = 0.6$. We can observe that the bifurcation diagrams are very consistent with the Lyapunov exponent spectra.

From Figs. 3 and 4, it is clear that the circuit is chaotic for a very wide range of α and evolves into chaotic orbits from a doubling-period route. It has been observed that with increasing α, for $3 \leq \alpha < 5.9$, the first and second Lyapunov exponents almost equal zero, and the others are less than zero, so the circuit is in a periodic state, which corresponds to one or several lines in the bifurcation diagram. At $\alpha = 4.62$ and $\alpha = 5.65$, there are two periodic bifurcation points. System (5) always has only one positive Lyapunov exponent for $5.9 \leq \alpha \leq 14.9$, which indicates that the circuit exhibits chaotic behaviors. When $14.9 < \alpha \leq 18.1$ is satisfied, the first Lyapunov exponent $LE1$ is positive, whereas

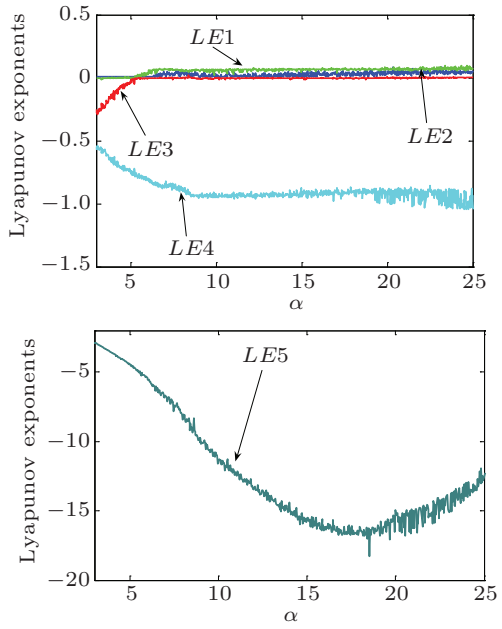


Fig. 3. (color online) The Lyapunov exponent spectra of system (5) with respect to α.

the second Lyapunov exponent $LE2$ is sometimes greater than zero and sometimes equals zero, implying that the circuit exhibits chaotic and hyperchaotic behaviors alternately. With $18.1 < \alpha \leq 25$, the first and second Lyapunov exponents are positive, and hence the circuit gradually evolves into a hyperchaotic state. Finally, the system equations show diverging behavior beyond $\alpha = 25.5$, indicating boundary crises. Several typical phase portraits of system (5) with different values of α are also shown in Fig. 5, which clearly portrays a period doubling route to chaos.

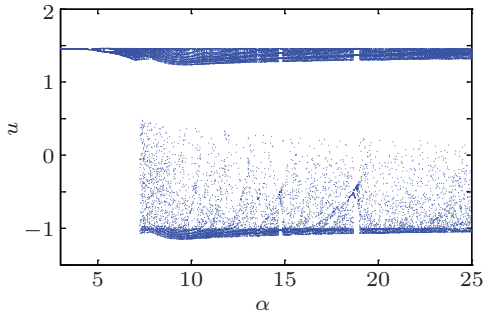


Fig. 4. (color online) Bifurcation diagram with respect to α.

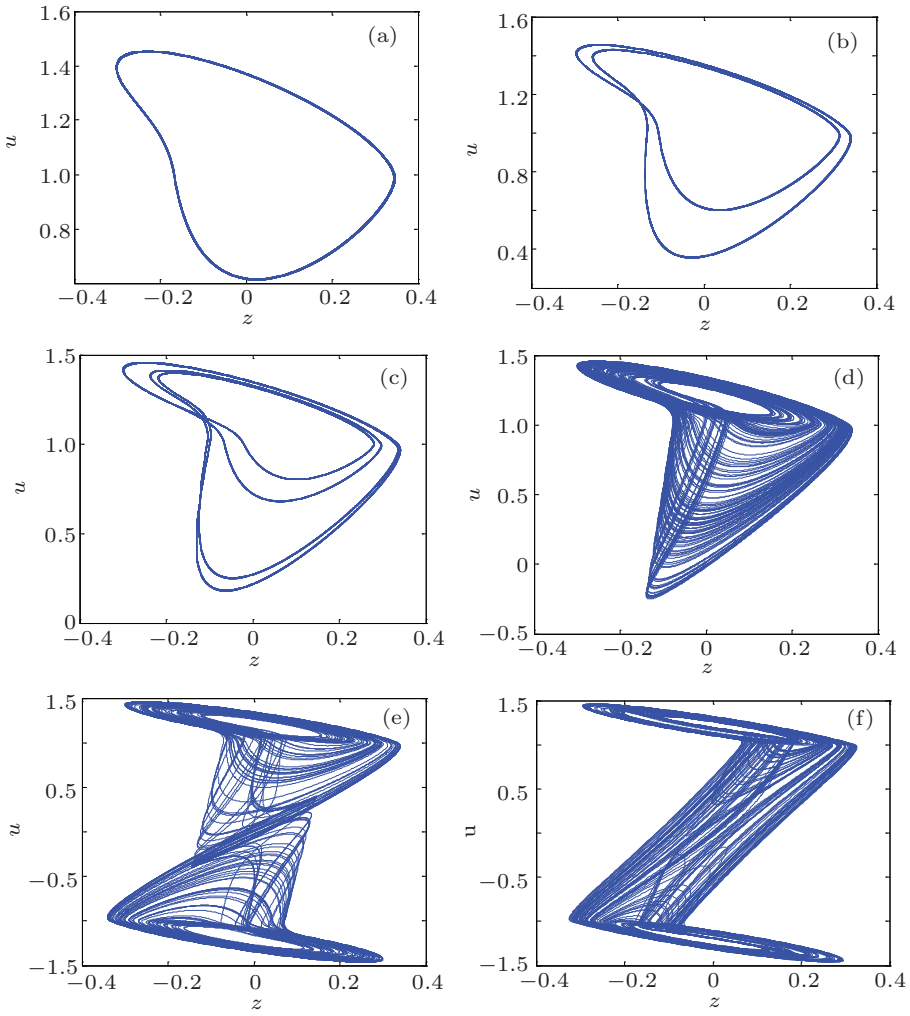


Fig. 5. (color online) Phase portraits in the z–u plane with different α: (a) $\alpha = 3.5$ (period-1), (b) $\alpha = 5$ (period-2), (c) $\alpha = 5.7$ (period-4), (d) $\alpha = 7$ (spiral chaos), (e) $\alpha = 7.8$ (double scroll), and (f) $\alpha = 22$ (hyperchaos).

From the above numerical simulation results, it is shown that the proposed circuit has very rich dynamics, such as periodic orbits, chaos, hyperchaos, and diverging behavior as α varies. Whereas hyperchaotic behavior cannot be found in similar circuits.[11–16] Moreover, the parameter range of the system (for $5.65 < \alpha < 25.5$) over which chaos exists is far wider than that of the other memristor circuit. Thus the proposed circuit has a capacity for dealing with a large domain of secret keys, which makes it suitable for implementing chaos-based imaging and real-time video encryption.

4. Pspice simulation

4.1. The emulator of the flux-controlled memristor

Since memristors are commercially unavailable, in order to create an experiment on the proposed circuit, we propose a simple analog realization of a piecewise linear flux-controlled memristor constructed with conventional electronic devices. The present emulator, shown in Fig. 6, is suitable for high-frequency chaos circuits due to a working frequency approximating to 30 kHz, which is far higher than that reported in Ref. [13].

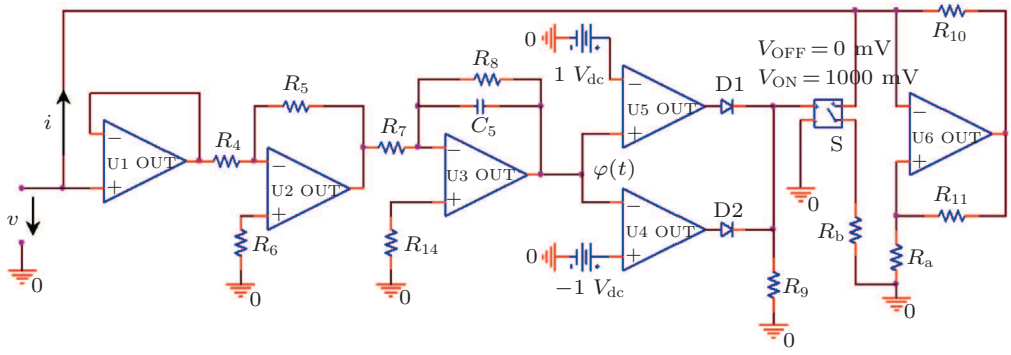


Fig. 6. (color online) The emulator of the flux-controlled memristor.

In Fig. 6, operational amplifier U3 is an integrator which converts the voltage across the memristor into the corresponding flux. A window comparator, constructed with U5 and U6, compares the flux across the memristor with two reference levels and hence controls the switch S to be on or off. U6 with resistors R_{10}, R_{11}, and R_a builds a negative impedance converter (NIC).[17] The operational process of the emulator can be explicitly depicted as follows: when the flux value across the memristor lies within the upper and lower reference levels, the switch S is "off" and only the negative conductance $-1/R_a$ is included in the circuit; for a flux value where the memristor exceeds the reference levels, the switch S turns on and hence the linear conductance R_b and the negative conductance $-1/R_a$, which are in parallel, are included in the circuit. So the conductance of the emulator can be given by

$$G(\varphi) = \begin{cases} -\dfrac{1}{R_a}, & \text{for } |\varphi| < 1, \\ \left(\dfrac{1}{R_b} - \dfrac{1}{R_a}\right), & \text{for } |\varphi| > 1. \end{cases} \tag{12}$$

Letting $a = -1/R_a$, and $b = (1/R_b - 1/R_a)$, the proposed emulator realizes the memductance of the memristor defined by Eq. (2) well.

4.2. Simulation results

With the aid of the proposed emulator, Pspice simulation experiments are conducted on the present chaotic circuit. The simulation results, shown in Fig. 7, are obtained with circuit parameters: $C_1 = C_2 = 0.5C_3 = C_0 = 4.7$ nF, $R_1 = R_2 = 2R_3 = R_0 = 5.7$ kΩ, $R_4 = 500$ Ω, $R_5 = 1000$ kΩ, $C_4 = 215$ pF, $R = 8.5$ kΩ, $R_a = 9.5$ kΩ, and $R_b = 4.75$ kΩ. In order to facilitate the observation, the corresponding phase planes obtained using numerical simulation for $\alpha = 22$, $k = 1.05$, $\gamma = 2/3$, $a = -0.6$, and $b = 0.6$, which correspond to the above mentioned circuit parameters, are also given in Fig. 7. Comparing the plots on the left (the Pspice simulation results) with the plots on the right (the numerical simulation results), we can observe that the phase portraits of the circuit variables are consistent with the corresponding phase portraits of the state variables in the numerical simulation. It is worth noting that figures 7(a) and 7(c) have some distortions, which result mainly from the integrator drift of the emulator. The characteristic of the emulator in the v–i plane is shown in Fig. 8. There is a pinched hysterectic curve, wherein the current falls to zero whenever the voltage across the memristor becomes zero. This is a characteristic feature of the memristors.

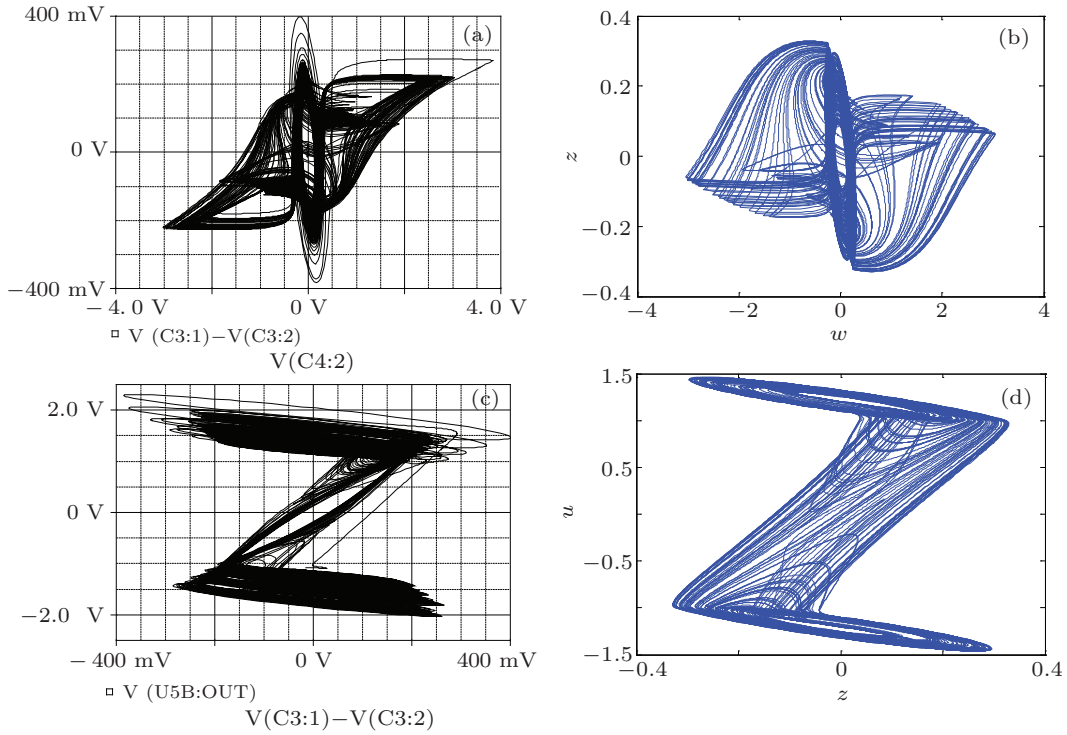


Fig. 7. Pspice simulation results versus numerical simulation results: (a) v_{C_4}–v_{C_3}, (b) w–z, (c) v_{C_3}–φ, (d) z–u.

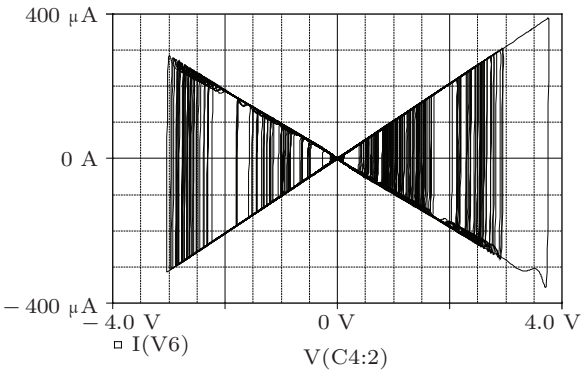


Fig. 8. The v–i phase portrait of the emulator.

5. Conclusions

In this work, an inductance-free chaotic circuit based on a twin-T oscillator and memristor is reported. The proposed circuit is modeled mathematically by five coupled first-order differential equations. By changing the control parameter, the circuit evolves into different orbits, chaos, and hyperchaos. Conventional dynamical analysis approaches, including equilibria stability, Lyapunov exponent spectra, and bifurcation diagrams, are conducted on the mathematical model of the circuit. In order to ensure the occurrence of chaos behaviors in the circuit, an analog realization of the piecewise-linear flux-controlled memristor is designed with conventional electronic devices. Pspice simulation results obtained with the aid of the emulator are in agreement with those from the theoretical analysis. The present circuit with no inductance is suitable for IC design and may be useful for chaos-based communication and electronic measurement systems.

References

[1] Chua L O 1971 *IEEE Trans. Circ. Theory* **CT-18** 507
[2] Chua L O and Kang S M 1976 *Proc. IEEE* **64** 209
[3] Strukov D B, Snider G S, Stewart D R and Williams R S 2008 *Nature* **453** 80
[4] Kavehei By O, Iqbal A, Kim Y S, Eshraghian K, Al-Sarawi S F and Abbott D 2010 *Proc. R. Soc. A* **466** 2175
[5] Pershin Y V, La Fontaine S and Di Ventra M 2009 *Phys. Rev. E* **80** 021926
[6] Borghetti J, Snider G S, Kuekes P J, Yang J J, Stewart D R and Williams R S 2010 *Nature* **464** 873
[7] Borghetti J, Li Z, Straznicky J, Li X, Ohlberg D A A, Wu W, Stewart D R and Williams R S 2009 *Proc. Natl. Ac. Sci.* **106** 1699
[8] Pershin Y V and Ventra M D 2010 *Neural Networks* **23** 881
[9] Jo S H, Chang T, Ebong I, Bhadviya B B, Mazumder P and Lu W 2010 *Nano Lett.* **10** 1297
[10] Driscoll T, Quinn J, Klein S, Kim H T, Kim B J, Pershin Y V, Ventra M Di and Basov D N 2010 *Appl. Phys. Lett.* **97** 093502
[11] Itoh M and Chua L O 2008 *Int. J. Bifur. Chaos* **18** 3183
[12] Muthuswamy B and Kokate P P 2009 *IETE Tech. Rev.* **26** 415
[13] Bao B C, Liu Z and Xu J P 2010 *Acta Phys. Sin.* **59** 3785 (in Chinese)
[14] Muthuswamy B 2010 *Int. J. Bifur. Chaos* **20** 1335
[15] Bao B C, Hu W, Xu J P and Liu Z 2011 *Acta Phys. Sin.* **60** 12052 (in Chinese)
[16] Liu Z, Bao B C and Xu J P 2010 *Chin. Phys. B* **19** 030510
[17] Yu S M and Yu Z D 2008 *Acta Phys. Sin.* **57** 6859 (in Chinese)